HHS Public Access

Author manuscript

Sci Immunol. Author manuscript; available in PMC 2020 July 24.

Published in final edited form as:

Sci Immunol. 2020 January 24; 5(43): . doi:10.1126/sciimmunol.aaz0085.

Mutual inhibition between Prkd2 and Bcl6 controls T follicular helper cell differentiation

Takuma Misawa[1,*], **Jeffrey A. SoRelle**[1], **Jin Huk Choi**[1], **Tao Yue**[1], **Kuan-wen Wang**[1], **William McAlpine**[1], **Jianhui Wang**[1], **Aijie Liu**[1], **Koichi Tabeta**[3], **Emre Turer**[1], **Bret Evers**[2], **Evan Nair-Gill**[1], **Subhajit Poddar**[1], **Lijing Su**[1], **Feiya Ou**[1], **Liyang Yu**[1], **Jamie Russell**[1], **Sara Ludwig**[1], **Xiaoming Zhan**[1], **Sara Hildebrand**[1], **Xiaohong Li**[1], **Miao Tang**[1], **Anne R. Murray**[1,†], **Eva Marie Y. Moresco**[1], **Bruce Beutler**[1,*]

[1]Center for the Genetics of Host Defense, UT Southwestern Medical Center, Dallas, TX 75390, USA.

[2]Division of Neuropathology, UT Southwestern Medical Center, Dallas, TX, 75390, USA.

[3]Division of Periodontology, Department of Oral Biological Science, Niigata University Graduate School of Medical and Dental Science, Niigata, Japan.

Abstract

T follicular helper cells (TFH) participate in germinal center (GC) development and are necessary for B cell production of high affinity, isotype switched antibodies. In a forward genetic screen we identified a missense mutation in *Prkd2*, encoding the serine/threonine kinase protein kinase D2, which caused elevated titers of IgE in the serum. Subsequent analysis of serum antibodies in mice with a targeted null mutation of *Prkd2* demonstrated polyclonal hypergammaglobulinemia of IgE, IgG1, and IgA isotypes, which was exacerbated by the T cell-dependent humoral response to immunization. GC formation and GC B cells were increased in $Prkd2^{-/-}$ spleens. These effects were the result of excessive cell autonomous TFH development caused by unrestricted Bcl6 nuclear translocation in $Prkd2^{-/-}$ $CD4^+$ T cells. Prkd2 directly binds to Bcl6 and Prkd2-dependent phosphorylation of Bcl6 is necessary to constrain Bcl6 to the cytoplasm, thereby limiting TFH development. In response to immunization, Bcl6 repressed *Prkd2* expression in $CD4^+$ T cells, thereby committing them to TFH development. Thus, Prkd2 and Bcl6 form a mutually inhibitory positive feedback loop that controls the stable transition from naïve $CD4^+$ T cells to TFH during the adaptive immune response.

One Sentence Summary:

[*]Corresponding authors: Takuma.Misawa@UTSouthwestern.edu, Bruce.Beutler@UTSouthwestern.edu.
[†]Current affiliation: Clinical Research Institute, Methodist Health System, Dallas, TX

Author contributions: Conceptualization: T.M., B.B.; Data curation: T.M., B.B.; Formal analysis: T.M., B.B.; Funding acquisition: T.M., B.B.; Investigation: T.M., J.S., J.H.C., T.Y., K-W.W., W.M., J.W., A.L., K.T., E.T., B.E., E.NG. S.P., L.S., F.O., L.Y., B.B.; Methodology: T.M., B.B.; Project administration: T.M., B.B., Resources: T.M., J.R., S.L., X.Z., S.H., X.L., M.T., B.B.; Software: B.B.; Supervision: B.B.; Validation: T.M., B.B.; Visualization: T.M., E.M.Y.M., B.B.; Writing- original draft: T.M., A.R.M., E.M.Y.M., B.B.; Writing- review and editing: T.M., E.M.Y.M., B.B.

Competing interests: The authors declare that they have no competing interests.

Data and materials availability: All data needed to evaluate the conclusions in the paper are present in the paper or the Supplementary Materials.

Prkd2-dependent phosphorylation of Bcl6 inhibits TFH cell differentiation.

Introduction

B cell activation by T helper (Th) cells initiates the humoral immune response to most protein antigens. Subsequently, T follicular helper cells (TFH) provide signals to B cells, including cytokines (IL-4, IFN-γ, IL-21) and cell surface ligands (ICOS, CD40L), to direct isotype switching and activate germinal center formation, somatic hypermutation, and affinity maturation (1-3) . Thus, impaired TFH can result in a limited or lower-affinity antibody response and consequent failure to control infections such as LCMV and HIV (4, 5), or to generate protective immunity in response to immunization (6, 7). Conversely, increased frequencies of TFH can facilitate autoantibody or IgE production, leading to autoimmune (8, 9) or allergic diseases (10-12), respectively. The development of TFH from naïve $CD4^+$ T cells (Th0) is subject to multiple regulatory mechanisms. The transcription repressor Bcl6 and other transcription factors downregulate genes required for alternative Th fates and activate the expression of key molecules that specify TFH differentiation, such as CXCR5 and PD-1 (13, 14).

Here, we show that excessive TFH development, GC formation, GC B cell activation, and antibody production are caused by mutations of *Prkd2*. The encoded protein, Prkd2, is one of three serine/threonine protein kinase D family isoforms in mammals, and has been most studied with respect to its role in multiple types of cancer (15, 16). In addition, it has been implicated in proinflammatory cytokine production by antigen-activated T cells (17-19). $Prkd2^{-/-}$ mice developed anti-DNA antibodies with age. We show evidence that Prkd2 and Bcl6 inhibit each other, thereby forming a mutually inhibitory positive feedback loop sensitive to antigen exposure, with implications for TFH fate determination.

Results

A Prkd2 mutation causes elevated serum antibodies

Using the chemical germline mutagen *N*-ethyl-*N*-nitrosourea (ENU), we mutated approximately 29.2% of all mouse protein coding genes to a state of phenovariance and tested these mutations three times or more in the homozygous state in a screen for aberrant IgE levels in serum in response to immunization with alum-precipitated ovalbumin (OVA/alum) (20). In all, 125,073 coding/splicing changes, distributed among 65,374 mice from 2,285 pedigrees were tested for phenotypic effects.

A mutation in *Prkd2*, named *Purnama* (20), was associated with increased serum concentrations of total and OVA-specific IgE after OVA/alum challenge (Fig. 1A, B). The $Prkd2^{Pur}$ mutation resulted in a tryptophan to arginine substitution at amino acid 807 (p.W807R) within the Prkd2 kinase domain. We recreated the *Purnama* mutation ($Prkd2^{W807R}$) in mice by utilizing CRISPR/Cas9 gene targeting. $Prkd2^{W807R/W807R}$ mice exhibited excessive production of IgE in response to OVA/alum (Fig. S1A, B). Moreover, expression of $Prkd2^{W807R}$ protein was significantly lower than that of wild-type Prkd2 when overexpressed in HEK293T cells (Fig. S1C). The IgE phenotype in *Purnama* mutants was

not limited to the response to OVA/alum as they produced IgE in excess after immunization with another model allergen, papain (Fig. S2A). *Prkd2* encodes an 875-amino acid serine/threonine kinase most highly expressed in the spleen, lymph node, thymus, and lung among those tissues examined (Fig. S3A). In the spleen, T cells and B cells expressed Prkd2, with higher levels of expression by T cells compared to B cells (Fig. S3B). We also generated a null allele of *Prkd2* (*Prkd2*$^{-/-}$) with CRISPR/Cas9 gene targeting, which recapitulated the elevated total and antigen-specific IgE production in heterozygous and homozygous mice (Fig. 1C, D, Fig. S2B, C). Further examination of total antibody levels in the serum of *Prkd2*$^{-/-}$ mice showed aberrantly elevated basal levels of IgE (Fig. 1C), IgA (Fig. 1E), IgM (Fig. 1F), and IgG1 (Fig. 1G), which were further increased following OVA/alum immunization (Fig. 1C-G). Total IgG2b was also slightly increased both before and after immunization in *Prkd2*$^{-/-}$ mice (Fig. 1H). In contrast, serum concentrations of IgG2a (Fig. 1I), IgG2c (Fig. 1J), and IgG3 (Fig. 1K) were similar in *Prkd2*$^{+/-}$, *Prkd2*$^{-/-}$, and wild-type mice irrespective of immunization.

Major immune cell populations were present at normal frequencies in the spleens of *Prkd2*$^{-/-}$ mice (Fig. S3C-K), suggesting that their development occurs normally. To test whether the increased antibody production observed in *Prkd2*$^{-/-}$ mice was due to the function of hematopoietic cells, we performed bone marrow (BM) transplantation. Irradiated *Rag2*$^{-/-}$ recipient mice engrafted with *Prkd2*$^{-/-}$ BM displayed elevated serum antibodies compared to *Rag2*$^{-/-}$ mice engrafted with *Prkd2*$^{+/+}$ BM, both before (IgA and IgM) and after (IgE, IgG1, IgA, and IgM) OVA/alum challenge (Fig. 1L-P), indicating that deficiency of Prkd2 in the hematopoietic compartment is sufficient to cause excessive antibody production. Using T cell receptor alpha knockout (*Tcra*$^{-/-}$) mice, we confirmed that except for IgM production, the altered antibody production in *Prkd2*$^{-/-}$ mice was T cell-dependent (Fig. S3L-P). In summary, loss-of-function mutations in *Prkd2* result in excessive T cell-dependent production of IgE, IgG1, and IgA.

Excessive cell autonomous TFH development occurs in Prkd2$^{-/-}$ mice

IL-4, produced by both Th2 and TFH, induces the expression of activation-induced cytidine deaminase and subsequent antibody isotype switching to IgE and IgG1 (21, 22). We found that *Prkd2*$^{-/-}$ CD4^{+} T cells produced significantly more IL-4 than *Prkd2*$^{+/+}$ CD4^{+} T cells when stimulated with PMA/ionomycin or anti-CD3/CD28 antibodies *in vitro* (Fig. 2A, B). In addition, flow cytometric analysis of cells from *Prkd2*$^{-/-}$ mice crossed to *Il4* reporter mice that contain a bicistronic IRES-EGFP reporter cassette inserted in the endogenous *Il4* locus (known as *4-get* mice) (23) showed greater percentages of GFP-expressing CD4^{+} T cells in *Prkd2*$^{-/-}$ spleens compared to *Prkd2*$^{+/+}$ spleens (Fig. 2C). We therefore hypothesized that Prkd2 deficiency leads to the enhanced development of Th2 or TFH. In support of enhanced TFH development, flow cytometric quantification of TFH (CXCR5^{high}PD-1^{high}CD4^{+}) in spleens and lymph nodes of *Prkd2*$^{-/-}$ mice revealed significantly increased frequencies and numbers compared to TFH in *Prkd2*$^{+/+}$ mice (Fig. 2D, Fig. S4A-C, Fig. S5). Consistent with the increased TFH numbers, frequencies and numbers of GC B cells and GC formation were also elevated in *Prkd2*$^{-/-}$ mice, even without immunization (Fig. 2E, F, Fig. S4A, D, E). The frequency of plasma cells was also significantly higher in bone marrow from *Prkd2*$^{-/-}$ mice than in *Prkd2*$^{+/+}$ mice (Fig. 2G).

In contrast, expression of the Th2-inducing transcription factors GATA3 and STAT6 (24) was comparable in *Prkd2*$^{-/-}$ and *Prkd2*$^{+/+}$ CD4^{+} T cells (Fig. S6A). Moreover, when CD4^{+} T cells were cultured *in vitro* under Th2-polarizing conditions, a smaller percentage of *Prkd2*$^{-/-}$ cells than *Prkd2*$^{+/+}$ cells induced IL-4 expression after PMA/ionomycin stimulation (Fig. S6B). Indeed, there was an increased percentage of IL-4^{+} TFH and a reduced percentage of IL-4^{+} Th2 in *Prkd2*$^{-/-}$ spleens compared to *Prkd2*$^{+/+}$ spleens, resulting in a greatly increased ratio of TFH to Th2 cells among IL-4-expressing CD4^{+} T cells in *Prkd2*$^{-/-}$ spleens compared to that in *Prkd2*$^{+/+}$ spleens (Fig. 3A, B). These data indicate that an overabundance of TFH exist in *Prkd2*$^{-/-}$ mice.

The transcriptional repressor Bcl6 plays a critical role in the development of TFH (25-30). Bcl6-deficient T cells fail to develop into TFH and sustain germinal center responses. Using *Prkd2*$^{-/-}$ mice conditionally lacking Bcl6 in CD4^{+} T cells (*Prkd2*$^{-/-}$Bcl6$^{fl/fl}$CD4-Cre^{+}), which have no TFH (Fig. S7A), we confirmed that the elevated frequencies of GC B cells (Fig. S7B) and increased serum concentrations of IgE (Fig. S7C, D), IgG1 (Fig. S7E), and IgA (Fig. S7F) in *Prkd2*$^{-/-}$ mice were TFH-dependent. Interestingly, we observed that specific deletion of *Bcl6* in wild-type CD4^{+} T cells resulted in elevated IgM production (Fig. S7G).

We next assessed the intrinsic proliferative potential of *Prkd2*$^{-/-}$ TFH by transferring a mixture containing equal numbers of *Prkd2*$^{+/+}$ (CD45.1^{+}) and *Prkd2*$^{-/-}$ (CD45.2^{+}) BM cells into lethally irradiated *Rag2*$^{-/-}$ mice. As a result, *Prkd2*$^{-/-}$ TFH expanded more robustly than *Prkd2*$^{+/+}$ TFH, resulting in an increased frequency of *Prkd2*$^{-/-}$ TFH compared to *Prkd2*$^{+/+}$ TFH in the spleens of recipient mice (Fig. 3C). We observed a similar effect when naïve CD4^{+} T cells (CD3^{+}CD4^{+}CD62L^{high}CD44^{low}) were adoptively transferred into *Rag2*$^{-/-}$ mice (Fig. 3D). These data indicate that *Prkd2*$^{-/-}$ TFH have a cell intrinsic proliferative advantage compared to wild-type TFH.

It was previously reported that CD4^{+} T cells from Prkd2 mutant mice, in which Ser707 and Ser711 were mutated to alanine within the Prkd2 kinase domain activation loop, exhibited reduced ability to produce IL-2 (17), a negative regulator of TFH development (31, 32). However, we found that IL-2 production by *Prkd2*$^{-/-}$ naïve CD4^{+} T cells was comparable to that of *Prkd2*$^{+/+}$ naïve CD4^{+} T cells when stimulated *in vitro* (Fig. S8A). Furthermore, frequencies of Th17 and Treg cells, Th cell subsets negatively or positively regulated by IL-2 (33), respectively, were unaffected or slightly increased in *Prkd2*$^{-/-}$ mice (Fig. S8B, C). Therefore, neither IL-2 production nor IL-2-regulated immune cells were affected by Prkd2 deficiency.

Excessive GC B cell development in Prkd2$^{-/-}$ mice is TFH-dependent

Bcl6 is also a key regulator of GC B cell development (34). Bcl6 mean fluorescence intensity (MFI) in *Prkd2*$^{-/-}$ GC B cells was lower than that in the corresponding *Prkd2*$^{+/+}$ cells (Fig. S9A). On the other hand, consistent with increased numbers of GC B cells in *Prkd2*$^{-/-}$ mice, frequencies of splenic Bcl6 expressing B cells were higher in *Prkd2*$^{-/-}$ mice than in *Prkd2*$^{+/+}$ mice (Fig. S9B). Similar to GC B cells, Bcl6 MFI in *Prkd2*$^{-/-}$ total B cells was lower than that in the corresponding *Prkd2*$^{+/+}$ cells (Fig. S9C). To test the effect of B cell-intrinsic Prkd2 deficiency on GC B cell development, we analyzed GC B cells in

Rag2$^{-/-}$ mice engrafted with equal numbers of *Prkd2*$^{+/+}$ (CD45.1^{+}) and *Prkd2*$^{-/-}$ (CD45.2^{+}) BM cells. We found that in the resulting chimeras, frequencies of *Prkd2*$^{-/-}$ GC B cells were comparable to that of *Prkd2*$^{+/+}$ GC B cells (Fig. S10A). We also generated bone marrow chimeras in which *Prkd2*$^{-/-}$ B cells developed in the presence of *Prkd2*$^{+/+}$ TFH (Fig. S10B, C). We adoptively transferred *Prkd2*$^{+/+}$*muMT* BM (as a donor of *Prkd2*$^{+/+}$ T cells) together with either *Prkd2*$^{+/+}$*Tcra*$^{-/-}$ BM (*Prkd2*$^{+/+}$ B cell donor) or *Prkd2*$^{-/-}$*Tcra*$^{-/-}$ BM (*Prkd2*$^{-/-}$B cell donor) into lethally irradiated *Rag2*$^{-/-}$ mice, and analyzed GC B cells. In the presence of *Prkd2*$^{+/+}$ T cells, the frequencies of GC B cells that developed were comparable between *Prkd2*$^{+/+}$ B cells and *Prkd2*$^{-/-}$ B cells (Fig. S10D, E). Moreover, IgE, IgG1, and IgA were normally produced by *Prkd2*$^{-/-}$ B cells with help from *Prkd2*$^{+/+}$ TFH (Fig. S10F-I). Collectively, these findings strongly suggest that excessive differentiation of *Prkd2*$^{-/-}$ GC B cells is a consequence of Prkd2 deficiency in TFH, and not due to cell intrinsic defects of *Prkd2*$^{-/-}$ B cells.

Prkd2-dependent phosphorylation of Bcl6 limits Bcl6 nuclear translocation in CD4^{+} T cells

Bcl6 MFI in *Prkd2*$^{-/-}$ TFH was slightly lower than in *Prkd2*$^{+/+}$ TFH (Fig. 4A). Consistent with increased numbers of TFH, frequencies of splenic Bcl6 expressing CD4^{+} T cells were higher in *Prkd2*$^{-/-}$ mice than in *Prkd2*$^{+/+}$ mice (Fig. 4B). Bcl6 MFI in total CD4^{+} T cells was comparable between *Prkd2*$^{+/+}$ and *Prkd2*$^{-/-}$ total CD4^{+} T cells (Fig. 4C). In both wild-type and *Prkd2*$^{-/-}$ CD4^{+} T cells, Bcl6 was localized primarily in the nucleus (Fig. 4D). However, the amount of Bcl6 in nuclear fractions of *Prkd2*$^{-/-}$ CD4^{+} T cells was increased compared to that observed in *Prkd2*$^{+/+}$ CD4^{+} T cells. Conversely, when Bcl6 was co-transfected with Prkd2 in HEK293T cells, nuclear Bcl6 levels were reduced and cytoplasmic Bcl6 levels were increased (Fig. 4E). Notably, both mouse and human Prkd2 exhibited similar effects on the subcellular localization of Bcl6. These findings suggest that Prkd2 limits the nuclear translocation of Bcl6 in CD4^{+} T cells.

We examined the possible interaction between Prkd2 and Bcl6 by co-transfecting tagged versions of both proteins into HEK293T cells. Prkd2 interacted with Bcl6 in reciprocal coimmunoprecipitation experiments (Fig. 4F, G). *In vitro* pull-down experiments using purified tagged recombinant proteins supported a direct interaction between Prkd2 and Bcl6 (Fig. 4H). We next examined the phosphorylation state of Bcl6 in the presence of Prkd2 in HEK293T cells using phosphate-affinity (Phos-tag) PAGE, in which the phosphorylated form of Bcl6 can be separated as a slower migrating band from non-phosphorylated Bcl6. A phosphorylated form of Bcl6 was observed when it was co-expressed with wild-type Prkd2, but not when it was co-expressed with a kinase-inactive form of Prkd2 lacking the kinase domain (Fig. 4I). Furthermore, kinase-inactive Prkd2 failed to suppress nuclear translocation of Bcl6 (Fig. 4J). These data suggest that an interaction between Bcl6 and Prkd2 leads to Bcl6 phosphorylation, either directly by Prkd2 or via a Prkd2 kinase-dependent event, thereby limiting Bcl6 access to the nucleus.

Collectively, our data indicate that Prkd2 deficiency derestricts Bcl6 nuclear translocation in CD4^{+} T cells resulting in excessive cell autonomous TFH development, and consequently leading to increased GC formation and activation/proliferation of B cells. These TFH, by virtue of their increased numbers and their increased propensity to produce IL-4 when

stimulated, are likely responsible for excessive IL-4 levels and ultimately excessive IgE, IgG1, and IgA production in *Prkd2*$^{-/-}$ mice.

Bcl6 downregulates Prkd2 in CD4^{+} T cells

TFH expand in response to antigenic challenge, for example during infection, and we hypothesized that Prkd2 levels or activity may be dynamically regulated to permit full expansion of TFH during an immune response. As expected to support such TFH development, both frequencies of Bcl6-expressing CD4^{+} T cells and Bcl6 MFI in CD4^{+} T cells were increased in response to immunization of wild-type mice with OVA/alum (Fig. 5A-C). At the same time (6 days after immunization), Prkd2 expression was decreased in CD4^{+} T cells from immunized mice, both at the protein and mRNA levels (Fig. 5C). In addition, we found that splenic TFH isolated from wild-type mice displayed low levels of Prkd2 expression concomitant with high levels of Bcl6 expression relative to non-TFH (Fig. 5D, Fig. S11). Based on these data and evidence from transcription profiling experiments that *Prkd2* is a target of Bcl6 (35), we hypothesized that Bcl6 represses *Prkd2* expression in CD4^{+} T cells in response to immunization. Consistent with this hypothesis, neither Prkd2 mRNA nor protein levels were downregulated in CD4^{+} T cells isolated from *Prkd2*$^{+/+}$Bcl6$^{fl/fl}$CD4-Cre^{+} mice challenged with OVA/alum (Fig. 5E). These data suggest that Bcl6 represses Prkd2 expression in CD4^{+} T cells following immunization to promote the efficient expansion of TFH.

We were interested in the molecular signals that trigger the Bcl6-mediated downregulation of *Prkd2* in CD4^{+} T cells after immunization. Among various cytokines applied to naïve CD4^{+} T cells, we found that IL-12, which is known to promote Th1 differentiation (36), suppressed Prkd2 protein and mRNA expression in wild-type CD4^{+} T cells (Fig. S12A). Previous studies have demonstrated that IL-12 upregulates Bcl6 in CD4^{+} T cells (37, 38); consistent with this, Bcl6 expression was enhanced in naïve CD4^{+} T cells cultured *in vitro* with IL-12 (Fig. S12B). We therefore hypothesized that IL-12-driven Bcl6 expression downregulates *Prkd2* in CD4^{+} T cells. As expected, both frequencies of Bcl6-expressing CD4^{+} T cells and Bcl6 MFI in total CD4^{+} T cells were impaired in *Il12a*$^{-/-}$ mice (Fig. S12C, D). Bcl6 MFI was also lower in TFH from *Il12a*$^{-/-}$ mice than in TFH from *Il12a*$^{+/+}$ mice (Fig. S12E). Consistently, *Il12a*$^{-/-}$ mice exhibited reduced frequencies of TFH and GC B cells compared to wild-type mice (Fig. S12F, G). Moreover, IgE production was diminished in *Il12a*$^{-/-}$ mice compared to wild-type mice (Fig. S12H). However, we found that Prkd2 expression decreased in CD4^{+} T cells in response to immunization of *Il12a*$^{-/-}$ mice with OVA/alum, possibly because of remaining Bcl6 expression in *Il12a*$^{-/-}$ CD4^{+} T cells (Fig. S12I). These data suggest the importance of other factor(s), either alone or in addition to IL-12, for the Bcl6-mediated downregulation of Prkd2 in CD4^{+} T cells that leads to TFH development following immunization.

Older Prkd2$^{-/-}$ mice develop anti-DNA antibodies

The consequence of increases in TFH numbers and/or hypergammaglobulinemia is often autoimmunity (14). *PRKD2* has been identified in genome-wide association studies as a candidate gene in a risk region for primary sclerosing cholangitis (54, 55), an autoimmune disease characterized by inflammation of the bile ducts in the liver. PSC patients produce

elevated levels of anti-nuclear antibodies (56). In support of these reports, we detected higher titers of anti-double-stranded DNA (dsDNA) antibodies that developed with increasing age in *Prkd2*$^{-/-}$ mice compared to wild-type mice (Fig. 6A-D). In addition, lymph nodes were enlarged in *Prkd2*$^{-/-}$ mice, which is another sign of autoimmune disease (Fig. S14A). Bronchus-associated lymphoid tissues (BALT) were spontaneously formed in *Prkd2*$^{-/-}$ lungs (Fig. S14B, C). Although the function of BALT is incompletely understood, BALTs are frequently observed in patients with various autoimmune disorders or allergies (Fig. S14D, E). The data presented in this paper provide a plausible mechanistic explanation for these findings, namely that excessive TFH may drive autoantibody production in human and mice with deficiencies of *PRKD2*.

Discussion

Using an unbiased forward genetic approach, we have elucidated a previously unrecognized role for Prkd2 in limiting TFH-dependent antibody responses (Fig. S13). We propose that in resting CD4$^+$ T cells, Prkd2-dependent phosphorylation of Bcl6 limits Bcl6 access to the nucleus, thereby suppressing the development of TFH. Upon antigen challenge, Bcl6 is upregulated, stoichiometrically overcomes the inhibitory effect of Prkd2, and enters the nucleus to drive TFH differentiation. In addition, the surge of Bcl6 entering the nucleus serves another function, to repress *Prkd2* transcription, thereby irreversibly committing the cells to TFH differentiation. In this final differentiated state, a new equilibrium is attained in which Prkd2 may no longer be relevant, as suggested by the stable low level of Prkd2 expression detected in TFH (Fig. 5D). On the other hand, the finding that normal frequencies of *Prkd2*$^{-/-}$ GC B cells develop in the presence of *Prkd2*$^{+/+}$ T cells indicates the absence of a B cell intrinsic defect of Bcl6 signaling, and that the relationship between Prkd2 and Bcl6 in B cells is probably different from that in CD4$^+$ T cells. Plasma cell frequencies were elevated in bone marrow from *Prkd2*$^{-/-}$ mice consistent with their excessive serum Ig levels (Fig. 2G). Plasma cells develop from either GCs or extrafollicular foci, both of which are formed with help from TFH (2). Thus, we anticipate that excessive TFH development in *Prkd2*$^{-/-}$ mice may also induce an overabundance of extrafollicular foci that promote plasma cell differentiation and subsequent hypergammaglobulinemia.

Interestingly, it has been reported that CD4$^+$ T cells expressing a mutant form of Prkd2 with reduced kinase activity, in which Ser707 and Ser711 in the kinase domain activation loop were mutated to Ala (designated PKD2^{SSAA}), displayed reduced ability to produce IL-2, a negative regulator of TFH, when stimulated in vitro (17) . However, we observed that IL-2 production in naïve *Prkd2*$^{-/-}$ CD4$^+$ T cells was normal or even slightly enhanced, both in terms of the frequency of IL-2 expressing CD4$^+$ T cells induced and the IL-2 MFI of those cells. Based on the phenotypes of T cells and B cells in the *Prkd2*$^{-/-}$ mice described here, we speculate that the effect of the partially active PKD2^{SSAA} protein on T cells may be more complex than initially proposed. Indeed, we observed different effects on IL-2 production by CD4$^+$ T cells and serum Ig levels in our *Prkd2*$^{-/-}$ mice than reported for *PKD2*$^{SSAA/SSAA}$ mice. Thus, we hypothesize that PKD2^{SSAA} alters T cell and B cell signaling pathways in a manner distinct from complete deletion of protein expression.

Bistable signaling as observed between Prkd2 and Bcl6, is known as reciprocal negative feedback or mutual inhibitory positive feedback, and has been observed in numerous biological systems (39) ranging from bacterial operons (40) to bacteriophage (41, 42) to mammalian systems, including several involved in immunity (Notch and Delta; Cdc2-cyclinB and Wee1; Cdc28-Clb2 and Sic1) (43-45). In general, such systems act to assure ordered, directional, stable transition between two discrete steady states. In this case, at issue is the differentiation from $CD4^+$ Th0 to $CD4^+$ TFH, a transition that necessitates directionality and stability because of its critical role in driving adaptive immune responses. The perturbation that normally initiates the transition is immunization, leading to the hematopoietic cell-dependent production of cytokines that stimulate Bcl6 expression and in turn, TFH development. Several cytokines are known to produce these effects, including IL-6, IL-21, and IL-12 (14). Interestingly, that IL-12 by itself strongly drives Th1 development is well-established (36), but the mechanism(s) regulating TFH versus Th1 differentiation induced by IL-12 are incompletely understood (37, 46, 47). We found that in addition to stimulating Bcl6 expression, IL-12 treatment of naïve $CD4^+$ T cells *in vitro* downregulated *Prkd2* expression, suggesting that this cytokine may act as one input to the bistable Prkd2-Bcl6 switch that results in the stable TFH 'output' rather than the Th1 alternative. While it might be assumed that lack of IL-12 would accelerate type 2 immune responses, we instead found that $Il12a^{-/-}$ mice produced less IgE than $Il12a^{+/+}$ mice in response to OVA/alum immunization. We interpret this to be the result of impaired commitment to the TFH lineage. A previous study has demonstrated that IL-12 is produced in mice challenged with alum adjuvant alone (48). The ability of IL-12 to promote TFH development via a Bcl6-Prkd2 switch may explain in part how alum adjuvants preferentially induce type 2 immune responses.

To date, Prkd2 has been well studied in the context of cancer, where it has been reported to have both tumor promoting and inhibitory functions (15, 16). In a tumor promoting role, it has been linked to positive regulation of angiogenesis downstream of VEGF-A by signaling the HSP90β-mediated stabilization of Bcl6-associated zinc finger protein (BAZF, also known as 'B cell CLL/lymphoma 6, member B' [Bcl6b]), which leads to downregulation of Notch signaling (49, 50). BAZF and Bcl6 share several domains with highly similar amino acid sequences (51), and the two proteins heterodimerize, an event necessary for the transcriptional repressive activity of BAZF (52). BAZF has been reported to be required for naïve CD4+ T cell proliferation in response to TCR activation and may oppose the function of Bcl6 in this process (53). Together with our data, these reports suggest the possibility that BAZF signaling may also contribute to the Prkd2-dependent regulation of TFH development. Further studies will be necessary to test this and to understand the mechanism of regulation.

Materials and Methods

We originally identified Prkd2 as a negative regulator of IgE by performing an unbiased forward genetic screen in ENU-mutagenized mice. *Prkd2* targeted mice with a null mutation exhibited excessive cell autonomous differentiation of TFH cells and hypergammaglobulinemia, validated by bone marrow/naïve CD4+ T cell chimera experiments. Through cell and molecular biological approaches, we verified that Prkd2 and

Bcl6 form a mutually inhibitory positive feedback loop in CD4+ T cells to regulate TFH differentiation during the adaptive immune response. Detailed methods are described in section below. The investigators were not blinded when performing the experiments. Control and experimental groups were age matched. Males and females were used in these experiments. At least five mice were used for each experiment. All experiments were repeated at least three times.

Mice

Eight- to ten-week old pure C57BL/6J background males purchased from The Jackson Laboratory were mutagenized with N-ethyl-N-nitrosourea (ENU) as described previously (20). Mutagenized G0 males were bred to C57BL/6J females, and the resulting G1 males were crossed to C57BL/6J females to produce G2 mice. G2 females were backcrossed to their G1 sires to yield G3 mice, which were screened for phenotypes. Whole-exome sequencing and mapping were performed as described (20). C57BL/6.SJL (CD45.1; #002014) (57), *Rag2*$^{-/-}$ (#008449) (58), *Tcra*$^{-/-}$ (#002116) (59), *muMT* (#002288) (60), *Bcl6*$^{fl/fl}$ (#023727) (61), *Il12a*$^{-/-}$ (#002692) (62), *NZB/BINJ* (#000684) (63), *NZW/LacJ*, (#001058) (64) and *CD4-Cre* transgenic mice (#017336) (65) were purchased from The Jackson Laboratory. *4-get* reporter mice were purchased from genOway. *Prkd2*$^{-/-}$/*4-get*, *Prkd2*$^{-/-}$ *Tcra*$^{-/-}$, *Prkd2*$^{-/-}$ *Bcl6*$^{fl/fl}$*CD4*-Cre^{+}, and NZB/NZW F1 hybrid mice were generated by intercrossing mouse strains. Mice were housed in specific pathogen–free conditions at the University of Texas Southwestern Medical Center and all experimental procedures were performed in accordance with institutionally approved protocols.

Generation of Prkd2^{W807R} and Prkd2 null mice using CRISPR/Cas9 system

Female C57BL/6J mice were superovulated by injection of 6.5 U pregnant mare serum gonadotropin (PMSG; Millipore), followed by injection of 6.5 U human chorionic gonadotropin (hCG; Sigma-Aldrich) 48 hours later. The superovulated mice were subsequently mated overnight with C57BL/6J male mice. The following day, fertilized eggs were collected from the oviducts and *in vitro*–transcribed Cas9 mRNA (50 ng/μl) and Prkd2 small base-pairing guide RNA (50 ng/μl; Prkd2: 5'- TCTCAGCCACCCATGGTTAC -3') was injected into the cytoplasm or pronucleus of the embryos. For generation of the *Prkd2*^{W807R} mutation that recapitulated the original Purnama allele, the following homology directed repair template was also injected: atcaacaacctgttgcaggtgaagatgcgcaagcgctacagcgtggacaagtctctcagccacccaAGGttacaAgtgacgtaggaggggggcctagaggaggcggcagagctaggtctctaattggctgggtgagtggg (affected codon TGG>AGG, and a silent mutation caG>caA designed to remove the sgRNA target site are indicated with uppercase font). The injected embryos were cultured in M16 medium (Sigma-Aldrich) at 37°C in 5% CO_2. For the production of mutant mice, two-cell stage embryos were transferred into the ampulla of the oviduct (10–20 embryos per oviduct) of pseudo-pregnant Hsd:ICR (CD-1) female mice (Harlan Laboratories). Sequencing showed that the null allele contained a 7 bp deletion of sequence TACAGGT (the final 5 bp at the 3' end of exon 17 and the first 2 bp at the 5' end of intron 17); no Prkd2 protein expression was detected in T cells from *Prkd2*$^{-/-}$ mice (Fig. 4D).

Immunization and ELISA analysis of serum immunoglobulins

Mice were immunized i.p. with aluminum hydroxide absorbed ovalbumin (OVA/alum; 200 μg; Invivogen) or papain (500 μg; Sigma). Unless otherwise noted, sera were harvested before immunization on day 0 and on day 10 post-immunization. For G3 mice, sera were harvested on day 14 after immunization. For analysis of T cell or B cell populations, unimmunized mice or immunized mice on the indicated day after immunization were sacrificed and spleen or lymph node cells were isolated for flow cytometric analysis.

Blood was collected in MiniCollect Tubes (Mercedes Medical) and centrifuged at 1,500 × *g* to separate the serum. To measure serum antibody isotype levels (IgE, IgA, IgM, IgG1, IgG2a, IgG2b, IgG2c, IgG3), freshly isolated serum was subjected to sandwich Enzyme-Linked ImmunoSorbent Assay (ELISA) analysis. ELISA kits for IgE, IgA, IgM, IgG2c, and IgG3 were purchased from Invitrogen. ELISA kits for IgG1, IgG2a, and IgG2b were purchased from Bethyl. ELISA analysis was performed according to the manufacturer's instructions. For ELISA analysis of antigen-specific IgE, or double-stranded DNA-specific IgG, Nunc MaxiSorp flat-bottom 96-well microplates (Thermo Fisher Scientific) were coated with 10-20 μg/mL OVA, 10 μg/mL Papain, or 50 μg/mL ultra pure calf thymus DNA solution (Thermo Fisher Scientific) at 4°C overnight. Plates were washed four times with washing buffer (0.05% (v/v) Tween-20 in PBS) using a BioTek microplate washer then blocked with 1% (v/v) BSA in PBS for 1 hour at room temperature. Serum samples were added to the prepared ELISA plates. After 2 hours incubation, the plates were washed four times with washing buffer and then incubated with HRP-conjugated goat anti-mouse IgE, HRP-conjugated goat anti-mouse IgG, HRP-conjugated goat anti-mouse IgA, or HRP-conjugated goat anti-mouse IgM (SouthernBiotech) for 30-45 minutes at room temperature. Plates were washed four times with washing buffer then developed with SureBlue TMB Microwell Peroxidase Substrate and TMB Stop Solution (KPL). Absorbance was measured at 450 nm on a Synergy Neo2 Plate Reader (BioTek).

Bone marrow transplantation and naïve CD4$^+$ T cell adoptive transfer

To generate bone marrow chimeras, *Rag2*$^{-/-}$ mice were lethally irradiated with 13 Gy via gamma radiation (X-RAD 320, Precision X-ray Inc.). The mice were given intravenous injection of 4 × 106 bone marrow cells derived from the tibia and femurs of the respective donors. For 2 weeks post-engraftment, mice were maintained on antibiotics. To generate mixed bone marrow chimeras the same procedure was performed, except that equal numbers of bone marrow cells from each of the donor genotypes were mixed (2 × 10^6 cells from each genotype) and transferred into irradiated *Rag2*$^{-/-}$ mice intravenously. 8-12 weeks after bone marrow engraftment, the chimeras were euthanized to assess TFH and GC B cell development in spleen by flow cytometry, or antibody responses to OVA/alum immunization. Chimerism was assessed using congenic CD45 markers. Splenic T cells and B cells were isolated from *Rag2*$^{-/-}$ mice engrafted with *muMT* and *Tcra*$^{-/-}$ bone marrows. Cells were lysed and subjected to immunoblot analysis to examine their Prkd2 level.

To generate mixed naïve CD4$^+$ T cell chimeras, *Rag2*$^{-/-}$ mice were lethally irradiated with 13 Gy via gamma radiation as described above. Splenic naïve CD4$^+$ T cells were isolated. Equal numbers of *Prkd2*$^{+/+}$ and *Prkd2*$^{-/-}$ naïve CD4$^+$ T cells were mixed (1.5 × 10^6 cells

from each genotype) and transferred into irradiated *Rag2*$^{-/-}$ mice intravenously. 7 days after naïve CD4$^+$ T cell transfer, the chimeras were euthanized to assess TFH development in spleen by flow cytometry. Chimerism was assessed using congenic CD45 markers.

Flow cytometry and cell sorting

The following antibodies were used: FITC CD3ε (145-2C11), BV786 CD4 (RM4-5), BV421 CD5 (53-7.3), BV 510 CD8α (53-6.7), BV711 CD11c (HL3), PE CD19 (1D3), Alexa Fluor 700 CD19 (1D3), BUV395 CD19 (1D3), BV421 CD23 (B3B4), APC CD43 (S7), PE-CF594 CD44 (IM7), Alexa Fluor 700 CD45R (RA3-6B2), PE-CF594 CD45.2 (104), BV510 CD95 (Jo2), PE Bcl6 (K112-91), PE RORγT (Q31-378), Alexa Fluor 647 Foxp3 (MF23), FITC IgM (II/41), PerCP/Cy5.5 IgM (RMM-1), Alexa Fluor 647 T and B cell activation antigen (GL7), PE F4/80 (BM8.1), PE-Cy7 CD62L (MEL-14), and PE Mouse IgG1, κ isotype control were purchased from BD Bioscience; APC/Cy7 CD3e (145-2C11), BV605 CD11b (M1/70), PerCP/Cy5.5 CD21/CD35 (7E9), PE/Cy7 CD45.1 (A20), FITC CD45.1 (A20), PE CD138 (281-2), APC CXCR5 (L138D7), BV421 PD-1 (29F.1A12), BV421 IL-2 (JES6-5H4), PE IL-4 (11B11), APC/Cy7 IgD (11-26c.2a), and BV650 NK1.1 (PK136) were purchased from Biolegend; PE CD3e (145-2C11) was purchased from Invitrogen. Splenocytes or lymph node cells were incubated with purified anti-mouse CD16/CD32 (2.4G2; TONBO) in PBS containing 5% FCS for blocking on ice. The cells were then stained using a 1:100 dilution of the indicated fluorescence dye-labeled antibodies. Intracellular staining for cytokine was performed after using BD Cytofix/Cytoperm (BD Biosciences) according to the manufacturer's instructions. Intracellular staining for Bcl6, RORγT, and Foxp3 was performed after using Mouse Foxp3 Buffer Set (BD Biosciences) according to the manufacturer's instructions. The stained cells were analyzed using a BD LSRFortessa cell analyzer (BD Biosciences).

Splenic CD4$^+$ T cells were stained with anti-CD3, anti-CD4, anti-CXCR5, and anti-PD-1 as described above. CXCR5^{low}PD-1^{low} or CXCR5^{high}PD-1^{high} CD4$^+$ T cells were then sorted using BD FACSAria IIU (BD Biosciences).

Isolation of primary immune cells

Splenic immune cells were isolated with Naïve CD4$^+$ T Cell Isolation Kit (Miltenyi Biotech), CD4$^+$ T Cell Isolation Kit (Miltenyi Biotech), CD8a$^+$ T Cell Isolation Kit (Miltenyi Biotech), Pan B Cell Isolation Kit (Miltenyi Biotech), CD11b MicroBeads (Miltenyi Biotech), CD11c MicroBeads (Miltenyi Biotech), CD49b (DX5) MicroBeads (Miltenyi Biotech), Neutrophil Isolation Kit (Miltenyi Biotech) according to manufacturer's instructions. Purities were over 95% in all experiments tested by flow cytometry.

T cell stimulation in vitro

Splenic CD4$^+$ T cells or naïve CD4$^+$ T cells were isolated as described above. Cells were stimulated in vitro with Leukocyte Activation Cocktail with BD GolgiPlug (PMA/ionomycin) (BD Biosciences), Dynabeads Mouse T-Activator CD3/CD28 (Thermo Fisher Scientific), or plate bound anti-TCRβ (10 μg/ml) and anti-CD28 (1 μg/ml) for 12 to 72 hours according to the manufacturer's instructions. IL-4 level in supernatant was analyzed by mouse IL-4 ELISA kit (Thermo Fisher Scientific).

Differentiation of Th subsets in vitro

Naïve $CD4^+$ T cells isolated from spleens were cultured in 24 well plates coated with anti-TCRβ (10μg/ml) and anti-CD28 (1 μg/ml). For Th0 condition, cells were incubated in the presence of IL-2 (20 ng/ml). For Th1 condition, cells were incubated with IL-2 (20 ng/ml), IL-12 (10 ng/ml), and with or without anti-IL-4 (5 μg/ml). For Th2 condition, cells were incubated with IL-2 (20 ng/ml), IL-4 (10 ng/ml), and anti-IFN-γ (5 μg/ml). Medium was refreshed every two days and cells were harvested on day 4-6. In vitro differentiated Th2 cells were used on day 6 for stimulation with PMA/ionomycin, except that stimulation was for 6 hours. Cells were stained with PE IL-4 (11B11; Biolegend) and analyzed by flow cytometry.

Cell culture, plasmids, and transfections

HEK293T cells were cultured at 37°C in 5% CO_2 in Dulbecco's modified Eagle's medium (DMEM, Life Technology) containing 10% (vol/vol) FBS and 1% antibiotics (Life Technology). Full-length human or mouse Bcl6, full-length human Prkd2, or human kinase domain-deleted Prkd2 were cloned into pCMV HA_N vector (Addgene). These plasmids were deposited in Addgene along with maps and sequences (Addgene ID; 137850, 137851, 138410, and 138411). pcDNA3.1(+)-N-DYK containing full-length human or mouse Prkd2 or full-length human Bcl6 were purchased from Genescript. pcDNA3.1(+)-N-DYK containing human kinase domain-deleted Prkd2 were purchased from Genescript. Tryptophan 807 within mouse Prkd2 was replaced into Arginine by using Q5 site-directed mutagenesis kit (New England Biolabs) according to manufacturer's instruction and cloned into pcDNA3.1(+)-N-DYK. Transfection of plasmids was carried out using Lipofectamine 2000 (Life Technologies) according to the manufacturer's instructions. In some experiments, cells were treated with increasing concentration (0, 1, 5, 10 μM) of MG132 (Millipore) for 12 hours.

Immunoprecipitation and pulldown assay

HEK293T cells were harvested between 36 and 48 hours post-transfection and lysed with NP-40 lysis buffer (25 mM Tris–HCl pH 8.0, 150 mM NaCl, 1% (vol/vol) Nonidet P-40, and protease inhibitors) for 45 min at 4°C. Immunoprecipitation was performed using anti-FLAG M2 magnetic beads (Sigma). Whole cell lysates and immunoprecipitates were immunoblotted using FLAG M2 antibody (Sigma) and HA antibody (Sigma).

FLAG-tagged human Bcl6 was transfected into HEK293T cells. 36 hours after transfection, FLAG-tagged human Bcl6 was immunoprecipitated using anti-FLAG M2 magnetic beads. Beads were then incubated with recombinant human GST-tagged Prkd2 (Thermo Fisher Scientific) for 2 hours at 4°C. Beads were washed three times with NP-40 lysis buffer. Beads were incubated with 3× FLAG peptide (Sigma) for 30 minutes and eluted proteins were subjected to immunoblot analysis.

Immunoblot analysis

Cells were lysed with either NP-40 lysis buffer (25 mM Tris–HCl pH 8.0, 150 mM NaCl, 1% (vol/vol) Nonidet P-40, and protease inhibitors) or SDS lysis buffer (50 mM Tris-HCl pH 6.8, 1% (vol/vol) SDS, and 10 % (vol/vol) glycerol). Protein concentrations were

normalized by performing BCA protein assay (Pierce). Lysates were subjected to gel electrophoresis using NuPAGE 4-12% Bis-Tris gels (Life Technologies). After electrophoresis, proteins were transferred to nitrocellulose membranes (Bio-Rad). For Phos-tag PAGE, cell lysates were subjected to gel electrophoresis using precast polyacrylamide gels containing Phos-tag (SuperSep Phos-tag; Wako). After electrophoresis, proteins were transferred to polyvinylidene difluoride (PVDF) membranes using a Mini Trans-Blot Cell (BioRad).

Membranes were blocked with Tris-buffered saline containing 0.1% (v/v) Tween-20 and 5% (w/v) non-fat dry milk (LabScientific) for 1-2 hours at room temperature. Proteins were detected by incubating membranes with the following antibodies: anti-Prkd2 (EPR1495Y) (Abcam); anti-α-Tubulin (DM1A), anti-β-Actin (13E5), anti-GATA3 (D13C9), anti-Histone H3 (3H1), anti-STAT6 (D3H4), HRP-conjugated anti-Rabbit IgG, and HRP-conjugated anti-Mouse IgG (Cell Signaling Technology); anti-Bcl6 (K112-91) (BD Biosciences). The chemiluminescence signal was developed using Super Signal West Pico Chemiluminescent Substrate or Super Signal West Dura Extended Duration Substrate kit (Thermo Fisher Scientific) and detected with a G:Box Chemi XX6 system (Syngene). Signal intensity of bands were quantified by ImageJ.

Histology

Spleens were harvested, embedded in Tissue-Tek O.C.T. (Sakura; Finetek) and frozen at −80°C. Cryostat sections (8 μm in thickness) were prepared, air-dried, and fixed in ice-cold acetone for 5 minutes. Sections were blocked with 3% BSA-containing PBS (wt/vol) for 30 minutes. Sections were further blocked using Avidin/Biotin Blocking Kit (Vector labs) and stained with PNA-biotin (Vector) and FITC anti-IgD (Biolegend). Biotinylated antibodies were detected with streptavidin, Alexa Fluor 546 conjugated antibody (Thermo). Sections were mounted with ProLong Gold antifade reagent (Invitrogen). Images were captured with a Zeiss AxioImager M1 microscope. Lungs were fixed with 4% Paraformaldehyde (Santa Cruz) for 24 hours at 4°C and then embedded in paraffin. Sections were stained with hematoxylin and eosin (HE). Images were captured with a Leica Application Suite V4 (Leica).

Fractionation analysis

Subcellular compartments were fractionated using NE-PER Nuclear and Cytoplasmic Extraction Reagents (Thermo Fisher Scientific) according to the manufacturer's instructions.

Quantitative RT-PCR

Total RNA was isolated using the Quick-RNA MiniPrep Kit (Zymo Research). cDNA fragments were reverse transcribed using SuperScript III First-Strand Synthesis SuperMix for qRT-PCR (Thermo Fisher Scientific) according to the manufacturer's instructions. qPCR was performed using TaqMan probes for *Prkd2* (Thermo Fisher Scientific; Mm00626821_m1) or *GAPDH* (Thermo Fisher Scientific; Mm99999915_g1). Fluorescence from the TaqMan probe for the *Prkd2* or *GAPDH RNA* gene was detected using a StepOnePlus Real-Time PCR System (Applied Biosystems). Relative standard curve method was used for the quantification.

Statistical Analysis

The statistical significance of differences between groups was determined using the indicated statistical tests and GraphPad Prism software. Data are expressed as means ± SD. Differences with *P* values ≥ 0.05 were considered to be not significant (NS). All differences with *P* values < 0.05 were considered significant. *P* values are denoted by $*P < 0.05$, $**P < 0.01$, $***P < 0.001$.

Supplementary Material

Refer to Web version on PubMed Central for supplementary material.

Acknowledgments:

We thank to all members of Center for the Genetics of Host Defense for their assistance.

Funding: This work was supported by National Institutes of Health grant AI125581 (to B.B.), AI100627 (to B.B.), K08DK107886 (to E.T.), 5U01AI095542 (to E.T.), Japan Society for the Promotion Science Overseas Research Fellowship (to T.M.), Uehara Memorial Foundation Overseas Postdoctoral Fellowship (to T.M.), and Osamu Hayaishi Memorial Foundation Scholarship for Study Abroad (to T.M.).

References and Notes:

1. Crotty S, T Follicular Helper Cell Biology: A Decade of Discovery and Diseases. Immunity 50, 1132–1148 (2019). [PubMed: 31117010]
2. Roco JA et al., Class-Switch Recombination Occurs Infrequently in Germinal Centers. Immunity 51, 337–350.e337 (2019). [PubMed: 31375460]
3. Kawabe T et al., The immune responses in CD40-deficient mice: impaired immunoglobulin class switching and germinal center formation. Immunity 1, 167–178 (1994). [PubMed: 7534202]
4. Fahey LM et al., Viral persistence redirects CD4 T cell differentiation toward T follicular helper cells. J Exp Med 208, 987–999 (2011). [PubMed: 21536743]
5. Cubas RA et al., Inadequate T follicular cell help impairs B cell immunity during HIV infection. Nat Med 19, 494–499 (2013). [PubMed: 23475201]
6. Bentebibel SE et al., Induction of ICOS+CXCR3+CXCR5+ TH cells correlates with antibody responses to influenza vaccination. Sci Transl Med 5, 176ra132 (2013).
7. Duan Z et al., Genetic polymorphisms of CXCR5 and CXCL13 are associated with non-responsiveness to the hepatitis B vaccine. Vaccine 32, 5316–5322 (2014). [PubMed: 25077417]
8. Simpson N et al., Expansion of circulating T cells resembling follicular helper T cells is a fixed phenotype that identifies a subset of severe systemic lupus erythematosus. Arthritis Rheum 62, 234–244 (2010). [PubMed: 20039395]
9. Vinuesa CG et al., A RING-type ubiquitin ligase family member required to repress follicular helper T cells and autoimmunity. Nature 435, 452–458 (2005). [PubMed: 15917799]
10. Harada Y et al., The 3' enhancer CNS2 is a critical regulator of interleukin-4-mediated humoral immunity in follicular helper T cells. Immunity 36, 188–200 (2012). [PubMed: 22365664]
11. Kobayashi T, Iijima K, Dent AL, Kita H, Follicular helper T cells mediate IgE antibody response to airborne allergens. J Allergy Clin Immunol 139, 300–313 e307 (2017). [PubMed: 27325434]
12. Yao Y, Wang ZC, Yu D, Liu Z, Role of allergen-specific T-follicular helper cells in immunotherapy. Curr Opin Allergy Clin Immunol 18, 495–501 (2018). [PubMed: 30124489]
13. Crotty S, T follicular helper cell differentiation, function, and roles in disease. Immunity 41, 529–542 (2014). [PubMed: 25367570]
14. Vinuesa CG, Linterman MA, Yu D, MacLennan IC, Follicular Helper T Cells. Annu Rev Immunol 34, 335–368 (2016). [PubMed: 26907215]

15. Roy A, Ye J, Deng F, Wang QJ, Protein kinase D signaling in cancer: A friend or foe? Biochimica et biophysica acta. Reviews on cancer 1868, 283–294 (2017). [PubMed: 28577984]
16. Azoitei N, Cobbaut M, Becher A, Van Lint J, Seufferlein T, Protein kinase D2: a versatile player in cancer biology. Oncogene 37, 1263–1278 (2018). [PubMed: 29259300]
17. Matthews SA et al., Unique functions for protein kinase D1 and protein kinase D2 in mammalian cells. Biochem J 432, 153–163 (2010). [PubMed: 20819079]
18. Navarro MN et al., Protein kinase D2 has a restricted but critical role in T-cell antigen receptor signalling in mature T-cells. Biochem J 442, 649–659 (2012). [PubMed: 22233340]
19. Navarro MN, Feijoo-Carnero C, Arandilla AG, Trost M, Cantrell DA, Protein kinase D2 is a digital amplifier of T cell receptor-stimulated diacylglycerol signaling in naive CD8(+) T cells. Science signaling 7, ra99 (2014). [PubMed: 25336615]
20. Wang T et al., Real-time resolution of point mutations that cause phenovariance in mice. Proc Natl Acad Sci U S A 112, E440–449 (2015). [PubMed: 25605905]
21. Kim RJ et al., IL-4-induced AID expression and its relevance to IgA class switch recombination. Biochem Biophys Res Commun 361, 398–403 (2007). [PubMed: 17645870]
22. Kubo M, T follicular helper and TH2 cells in allergic responses. Allergol Int 66, 377–381 (2017). [PubMed: 28499720]
23. Mohrs K, Wakil AE, Killeen N, Locksley RM, Mohrs M, A two-step process for cytokine production revealed by IL-4 dual-reporter mice. Immunity 23, 419–429 (2005). [PubMed: 16226507]
24. Walker JA, McKenzie ANJ, TH2 cell development and function. Nat Rev Immunol 18, 121–133 (2018). [PubMed: 29082915]
25. Nurieva RI et al., Bcl6 mediates the development of T follicular helper cells. Science 325, 1001–1005 (2009). [PubMed: 19628815]
26. Liu X et al., Bcl6 expression specifies the T follicular helper cell program in vivo. J Exp Med 209, 1841–1852, S1841-1824 (2012). [PubMed: 22987803]
27. Yu D et al., The transcriptional repressor Bcl-6 directs T follicular helper cell lineage commitment. Immunity 31, 457–468 (2009). [PubMed: 19631565]
28. Johnston RJ et al., Bcl6 and Blimp-1 are reciprocal and antagonistic regulators of T follicular helper cell differentiation. Science 325, 1006–1010 (2009). [PubMed: 19608860]
29. Hatzi K et al., BCL6 orchestrates Tfh cell differentiation via multiple distinct mechanisms. J Exp Med 212, 539–553 (2015). [PubMed: 25824819]
30. Weinstein JS et al., TFH cells progressively differentiate to regulate the germinal center response. Nat Immunol 17, 1197–1205 (2016). [PubMed: 27573866]
31. Ballesteros-Tato A et al., Interleukin-2 inhibits germinal center formation by limiting T follicular helper cell differentiation. Immunity 36, 847–856 (2012). [PubMed: 22464171]
32. DiToro D et al., Differential IL-2 expression defines developmental fates of follicular versus nonfollicular helper T cells. Science 361, (2018).
33. Kim CH, Regulation of FoxP3 regulatory T cells and Th17 cells by retinoids. Clin Dev Immunol 2008, 416910 (2008). [PubMed: 18389070]
34. Basso K, Dalla-Favera R, BCL6: master regulator of the germinal center reaction and key oncogene in B cell lymphomagenesis. Adv Immunol 105, 193–210 (2010). [PubMed: 20510734]
35. Liu X et al., Genome-wide Analysis Identifies Bcl6-Controlled Regulatory Networks during T Follicular Helper Cell Differentiation. Cell Rep 14, 1735–1747 (2016). [PubMed: 26876184]
36. Szabo SJ et al., A novel transcription factor, T-bet, directs Th1 lineage commitment. Cell 100, 655–669 (2000). [PubMed: 10761931]
37. Nakayamada S et al., Early Th1 cell differentiation is marked by a Tfh cell-like transition. Immunity 35, 919–931 (2011). [PubMed: 22195747]
38. Schmitt N et al., IL-12 receptor beta1 deficiency alters in vivo T follicular helper cell response in humans. Blood 121, 3375–3385 (2013). [PubMed: 23476048]
39. Kim TH, Jung SH, Cho KH, Interlinked mutual inhibitory positive feedbacks induce robust cellular memory effects. FEBS Lett 581, 4899–4904 (2007). [PubMed: 17892872]

40. Jacob F, Monod J, Genetic regulatory mechanisms in the synthesis of proteins. J Mol Biol 3, 318–356 (1961). [PubMed: 13718526]
41. Oppenheim AB, Kobiler O, Stavans J, Court DL, Adhya S, Switches in bacteriophage lambda development. Annu Rev Genet 39, 409–429 (2005). [PubMed: 16285866]
42. Ptashne M, Lambda's switch: lessons from a module swap. Curr Biol 16, R459–462 (2006). [PubMed: 16782001]
43. Yuan JS, Kousis PC, Suliman S, Visan I, Guidos CJ, Functions of notch signaling in the immune system: consensus and controversies. Annu Rev Immunol 28, 343–365 (2010). [PubMed: 20192807]
44. Perry JA, Kornbluth S, Cdc25 and Wee1: analogous opposites? Cell Div 2, 12 (2007). [PubMed: 17480229]
45. Chen KC et al., Kinetic analysis of a molecular model of the budding yeast cell cycle. Mol Biol Cell 11, 369–391 (2000). [PubMed: 10637314]
46. Weinmann AS, Regulatory mechanisms that control T-follicular helper and T-helper 1 cell flexibility. Immunol Cell Biol 92, 34–39 (2014). [PubMed: 24080769]
47. Schmitt N, Liu Y, Bentebibel SE, Ueno H, Molecular Mechanisms Regulating T Helper 1 versus T Follicular Helper Cell Differentiation in Humans. Cell Rep 16, 1082–1095 (2016). [PubMed: 27425607]
48. McKee AS et al., Alum induces innate immune responses through macrophage and mast cell sensors, but these sensors are not required for alum to act as an adjuvant for specific immunity. J Immunol 183, 4403–4414 (2009). [PubMed: 19734227]
49. Miwa D et al., Protein kinase D2 and heat shock protein 90 beta are required for BCL6-associated zinc finger protein mRNA stabilization induced by vascular endothelial growth factor-A. Angiogenesis 16, 675–688 (2013). [PubMed: 23515950]
50. Ohnuki H et al., BAZF, a novel component of cullin3-based E3 ligase complex, mediates VEGFR and Notch cross-signaling in angiogenesis. Blood 119, 2688–2698 (2012). [PubMed: 22279058]
51. Okabe S et al., BAZF, a novel Bcl6 homolog, functions as a transcriptional repressor. Molecular and cellular biology 18, 4235–4244 (1998). [PubMed: 9632807]
52. Takenaga M et al., Bcl6-dependent transcriptional repression by BAZF. Biochem Biophys Res Commun 303, 600–608 (2003). [PubMed: 12659862]
53. Takamori M et al., BAZF is required for activation of naive CD4 T cells by TCR triggering. International immunology 16, 1439–1449 (2004). [PubMed: 15314041]
54. Ji SG et al., Genome-wide association study of primary sclerosing cholangitis identifies new risk loci and quantifies the genetic relationship with inflammatory bowel disease. Nat Genet 49, 269–273 (2017). [PubMed: 27992413]
55. Karlsen TH, Folseraas T, Thorburn D, Vesterhus M, Primary sclerosing cholangitis - a comprehensive review. J Hepatol 67, 1298–1323 (2017). [PubMed: 28802875]
56. Hov JR, Boberg KM, Karlsen TH, Autoantibodies in primary sclerosing cholangitis. World J Gastroenterol 14, 3781–3791 (2008). [PubMed: 18609700]
57. Janowska-Wieczorek A et al., Platelet-derived microparticles bind to hematopoietic stem/progenitor cells and enhance their engraftment. Blood 98, 3143–3149 (2001). [PubMed: 11698303]
58. Hao Z, Rajewsky K, Homeostasis of peripheral B cells in the absence of B cell influx from the bone marrow. J Exp Med 194, 1151–1164 (2001). [PubMed: 11602643]
59. Mombaerts P et al., Mutations in T-cell antigen receptor genes alpha and beta block thymocyte development at different stages. Nature 360, 225–231 (1992). [PubMed: 1359428]
60. Kitamura D, Roes J, Kuhn R, Rajewsky K, A B cell-deficient mouse by targeted disruption of the membrane exon of the immunoglobulin mu chain gene. Nature 350, 423–426 (1991). [PubMed: 1901381]
61. Hollister K et al., Insights into the role of Bcl6 in follicular Th cells using a new conditional mutant mouse model. J Immunol 191, 3705–3711 (2013). [PubMed: 23980208]

62. Mattner F et al., Genetically resistant mice lacking interleukin-12 are susceptible to infection with Leishmania major and mount a polarized Th2 cell response. Eur J Immunol 26, 1553–1559 (1996). [PubMed: 8766560]

63. Paigen B, Morrow A, Brandon C, Mitchell D, Holmes P, Variation in susceptibility to atherosclerosis among inbred strains of mice. Atherosclerosis 57, 65–73 (1985). [PubMed: 3841001]

64. Depis F, Kwon HK, Mathis D, Benoist C, Unstable FoxP3+ T regulatory cells in NZW mice. Proc Natl Acad Sci U S A 113, 1345–1350 (2016). [PubMed: 26768846]

65. Sawada S, Scarborough JD, Killeen N, Littman DR, A lineage-specific transcriptional silencer regulates CD4 gene expression during T lymphocyte development. Cell 77, 917–929 (1994). [PubMed: 8004678]

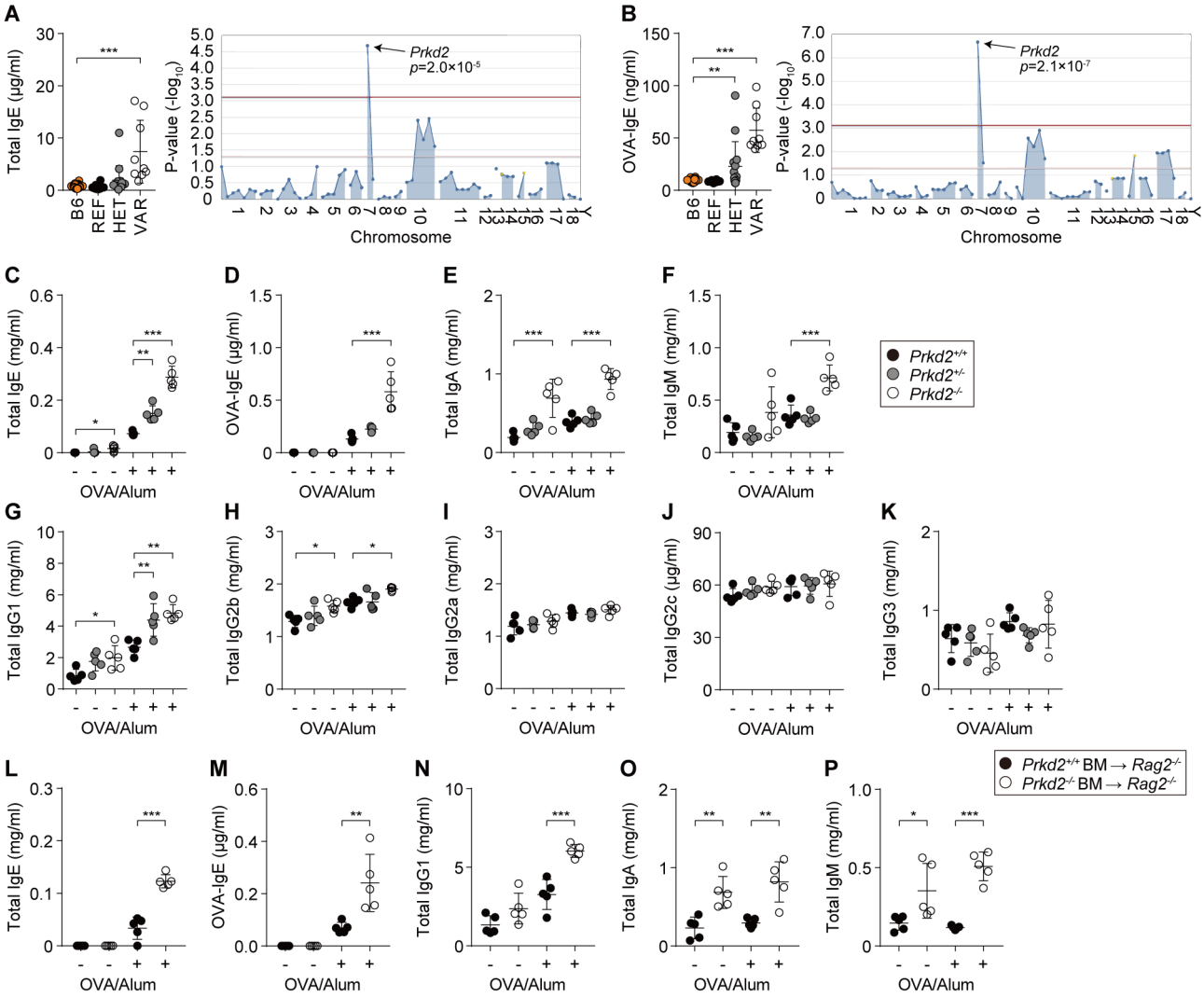

Fig. 1. Elevated serum IgE, IgG1, IgA, and IgM in Prkd2 deficient mice.

(**A, B**) Phenotypic screening data. Serum antibodies in mice on day 14 post-immunization with OVA/alum. (**A**) Total IgE and (**B**) OVA-specific IgE in wild-type C57BL/6J mice (B6), or the G3 descendants of a single ENU-mutagenized male mouse with REF (+/+), HET (*Purnama*/+), or VAR (*Purnama/Purnama*) genotypes for *Prkd2* (left). Manhattan plot showing the *P* values of association between the total IgE (**A**) or OVA-IgE phenotype (**B**) and mutations identified in the affected pedigree calculated using a recessive model of inheritance (right). $-Log_{10}$ *P*-values are plotted vs. the chromosomal positions of mutations. Horizontal red and purple lines represent thresholds of $P = 0.05$ with or without Bonferroni correction, respectively. The *P* values for linkage of the *Prkd2* mutation are indicated. (**C**-**P**) Serum antibodies were measured before immunization (−) and on day 10 post-immunization with OVA/alum (+). Total IgE (**C**), OVA-specific IgE (**D**), total IgA (**E**), total IgM (**F**), total IgG1 (**G**), total IgG2b (**H**), total IgG2a (**I**), total IgG2c (**J**), and total IgG3 (**K**) concentration in serum from $Prkd2^{+/+}$, $Prkd2^{+/-}$, and $Prdk2^{-/-}$ mice. (**L**-**P**) Total IgE (**L**), OVA-specific IgE (**M**), total IgG1 (**N**), total IgA (**O**), and total IgM (**P**) concentration in serum from $Rag2^{-/-}$ mice engrafted with $Prkd2^{+/+}$ or $Prkd2^{-/-}$ bone marrow. Each symbol represents an

individual mouse. Data are representative of three independent experiments with at least 5 mice/genotype (mean ± SD); *P* values were determined by one-way ANOVA with Tukey's multiple comparisons test (**A**-**K**) or unpaired Student's *t* test (**L**-**P**) (**P* < 0.05, ***P* < 0.01, and ****P* < 0.001).

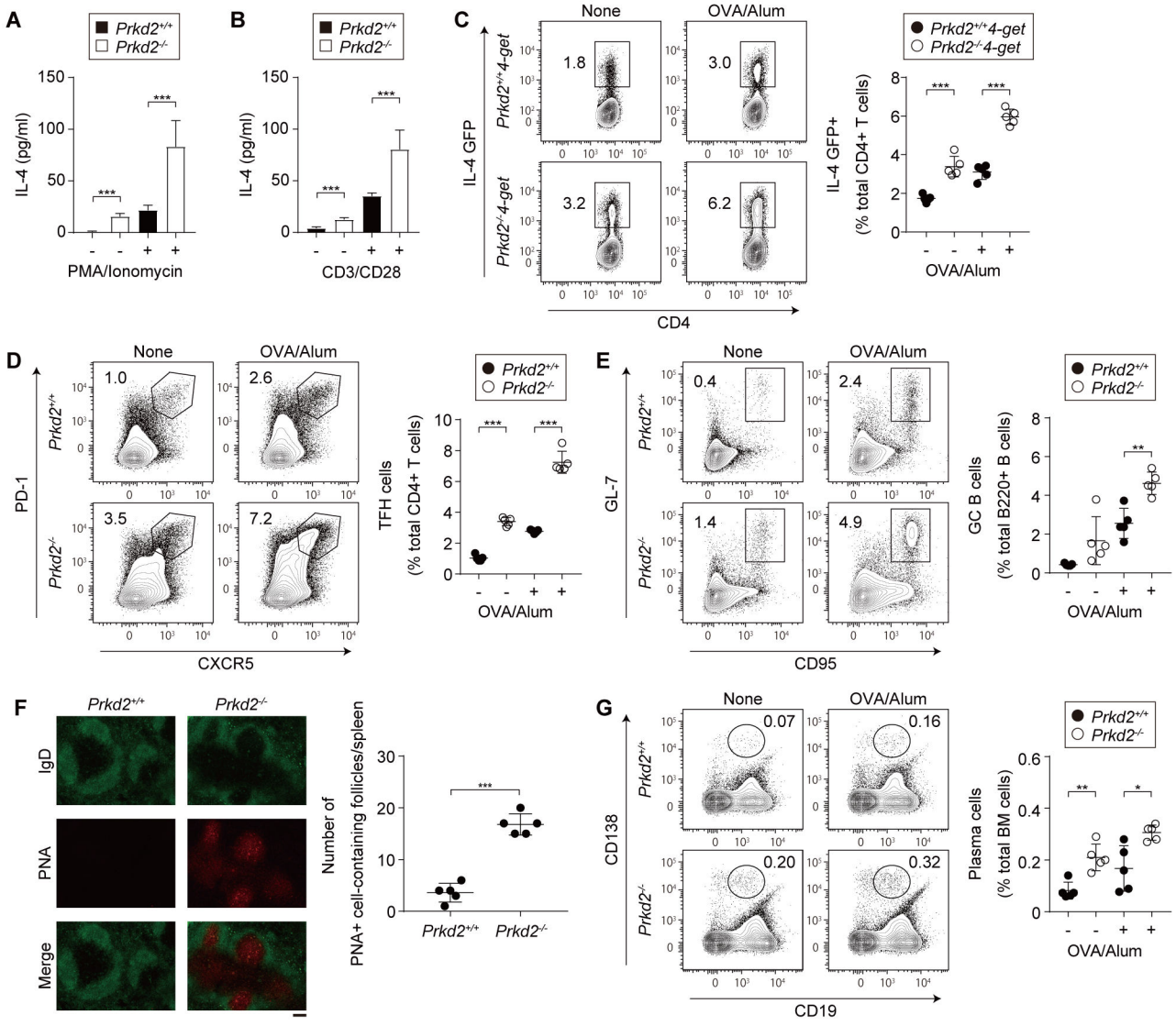

Fig. 2. Increased numbers of TFH and GC B cells in *Prkd2*$^{-/-}$ mice.

(**A, B**) IL-4 concentration in the culture medium of splenic CD4^{+} T cells left unstimulated (−) or stimulated (+) with PMA/ionomycin (**A**) or anti-CD3/CD28 coated beads (**B**) for 72 hours. N = 5 cultures from independent mice per genotype and condition. (**C-E**) The indicated cell populations were analyzed by flow cytometry in unimmunized mice (−) or in immunized mice on day 7 post-immunization with OVA/alum (+). (**C**) Representative flow cytometric scatter plots (left) and quantification (right) of the frequency of splenic IL-4-GFP^{high}CD4^{+} T cells (CD3^{+}CD4^{+}GFP^{high}) among CD4^{+} T cells. (**D, E**) Representative flow cytometric scatter plots (left) and quantification (right) of the frequency of splenic TFH cells (CD3^{+}CD4^{+}CXCR5^{high}PD-1^{high}) among CD4^{+} T cells (**D**), or germinal center B cells (CD3^{-}B220^{+}GL-7^{high}CD95^{high}) among B220^{+} cells (**E**). (**F**) Confocal images of spleen cryosections from unimmunized *Prkd2*$^{+/+}$ or *Prkd2*$^{-/-}$ mice (left). The sections were stained with anti-IgD (green) and peanut agglutinin (PNA; red). Scale bar, 100 μm. Quantification of number of follicles containing PNA^{+} cells per spleen (right). (**G**) Representative flow

cytometric scatter plots (left) and quantification (right) of the frequency of plasma cells ($CD19^{+}CD138^{high}$) in bone marrow. Numbers adjacent to outlined areas indicate percent cells in each (**C-E, G**). Each symbol represents an individual mouse (**C-G**). Data are representative of three independent experiments with at least 5 mice/genotype (mean ± SD); *P* values were determined by unpaired Student's *t* test (**P* < 0.05, ***P* < 0.01, and ****P* < 0.001).

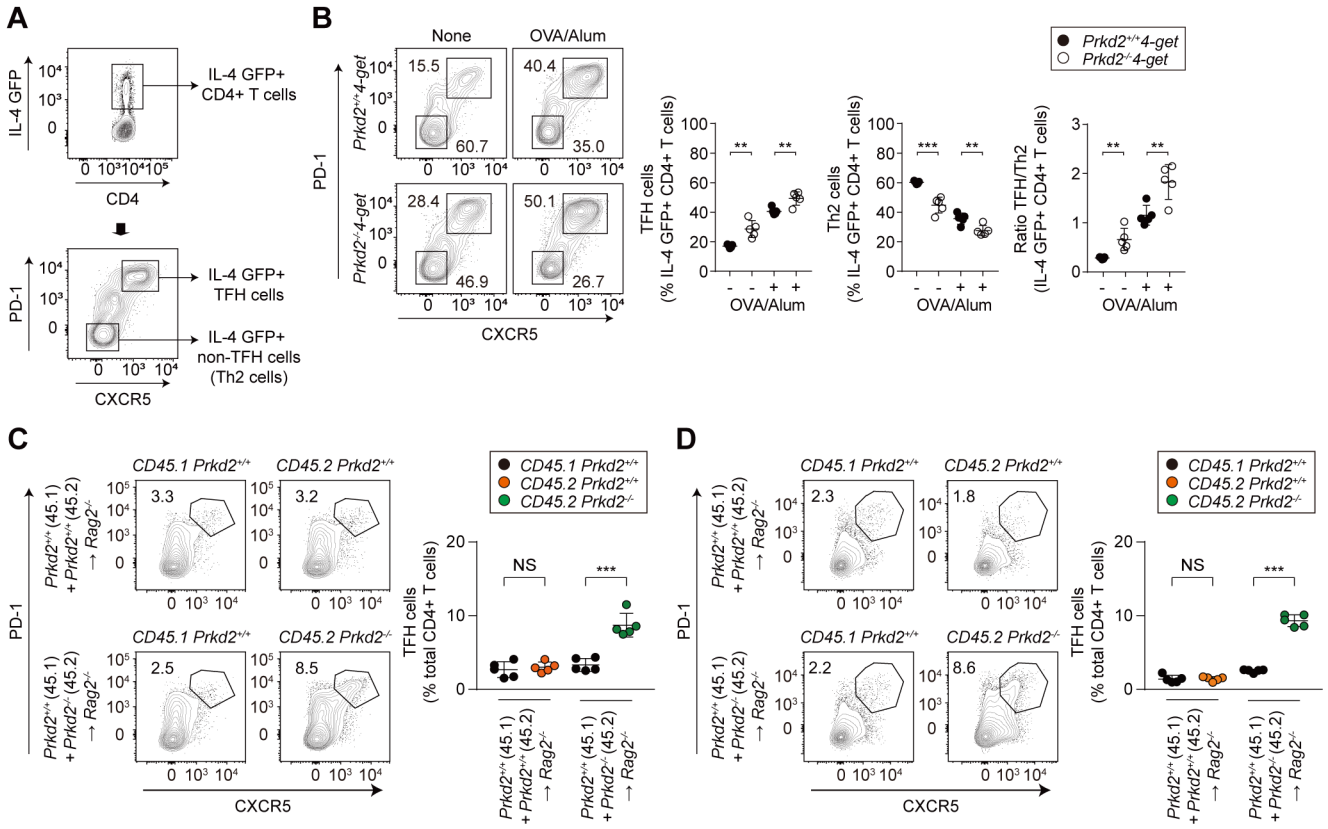

Fig. 3. Excessive cell autonomous *Prkd2*$^{-/-}$ TFH development.

(**A**) Flow cytometric gating strategy. Splenic IL-4-GFP^{+}CD4^{+} T cells (CD3^{+}CD4^{+}GFP^{high}) were analyzed using PD-1 and CXCR5 markers to detect IL-4-GFP^{+} TFH (PD-1^{high}CXCR5^{high}) and IL-4-GFP^{+} non-TFH (Th2) cells (PD-1^{low}CXCR5^{low}). (**B**) TFH and Th2 cells were analyzed by flow cytometry in unimmunized mice (−) or in immunized mice on day 7 post-immunization with OVA/alum (+). Representative flow cytometric scatter plots (left) and quantification (right) of the frequency of IL-4-GFP^{+} TFH and IL-4-GFP^{+} Th2 cells among splenic IL-4-GFP^{+}CD4^{+} T cells. Ratio between IL-4-GFP^{+} TFH and IL-4-GFP^{+} Th2 cells within GFP^{high}CD4^{+} T cells was also calculated. (**C, D**) Reconstitution of CD4^{+} T cells and TFH in spleens of irradiated *Rag2*$^{-/-}$ recipient mice engrafted with a mixture containing equal numbers of *Prkd2*$^{+/+}$ (CD45.1^{+}) and *Prkd2*$^{-/-}$ (CD45.2^{+}) bone marrow cells (**C**) or naïve CD4^{+} T cells (**D**). Representative flow cytometric scatter plots (left) and quantification (right) of the frequency of TFH cells (CD3^{+}CD4^{+}CXCR5^{high}PD-1^{high}) derived from each donor among CD4^{+} T cells (lower graphs). Quantification of the frequency of donor-derived CD4^{+} T cells (CD3^{+}CD4^{+}) in the spleen is also shown (upper graphs). Data are representative of three independent experiments with at least 5 mice/genotype (mean ± SD); *P* values were determined by unpaired Student's *t* test (NS: not significant, $^{**}P < 0.01$, and $^{***}P < 0.001$).

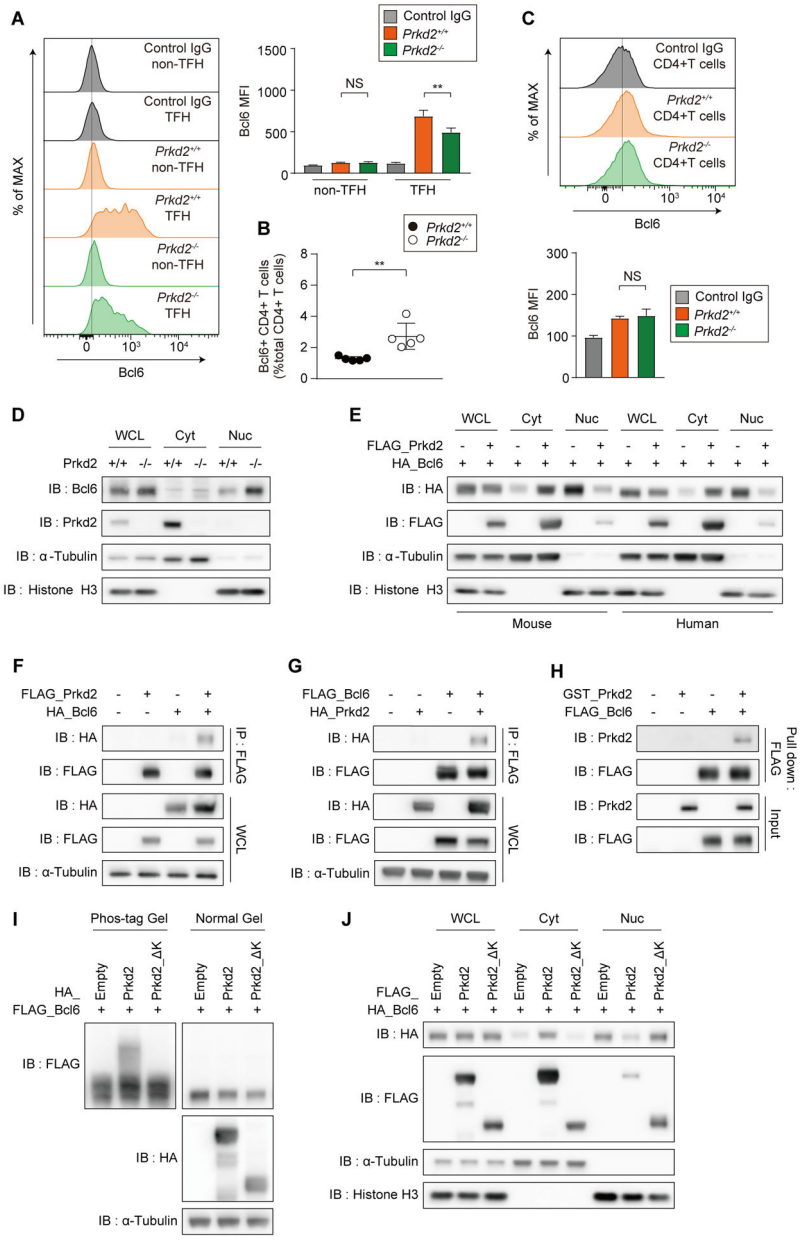

Fig. 4. Prkd2-dependent phosphorylation of Bcl6 limits Bcl6 access to the nucleus in CD4$^+$ T cells.

(**A**) Mean fluorescence intensity of Bcl6 in non-TFH ($CD3^+CD4^+PD\text{-}1^{low}CXCR5^{low}$) and TFH ($CD3^+CD4^+PD\text{-}1^{high}CXCR5^{high}$) in spleen. *Prkd2*$^{+/+}$ splenocytes were used to stain with isotype control IgG. Representative flow cytometric histogram plots (left) and quantification (right). (**B**) Frequency of Bcl6 expressing CD4$^+$ T cells ($CD3^+CD4^+Bcl6^{high}$) in spleen. (**C**) Mean fluorescence intensity of Bcl6 in splenic CD4$^+$ T ($CD3^+CD4^+$) cells. *Prkd2*$^{+/+}$ splenocytes were used to stain with isotype control IgG. Representative flow cytometric histogram plots (above) and quantification (below). (**D**) Immunoblot analysis of Bcl6 in whole cell lysates (WCL), cytosolic extracts (Cyt), or nuclear (Nuc) extracts of pooled CD4$^+$ T cells from *Prkd2*$^{-/-}$ or *Prkd2*$^{+/+}$ littermates. (**E**) Immunoblot analysis of HA-

tagged Bcl6 in whole cell lysates, cytosolic extracts, or nuclear extracts of HEK293T cells transfected with or without FLAG-tagged Prkd2. Mouse (left) and human proteins (right) are shown. (**F**) FLAG-tagged human Prkd2 was transfected into HEK293T cells with or without HA-tagged human Bcl6, and whole cell lysates were subjected to immunoprecipitation with anti-FLAG M2 magnetic beads, followed by immunoblotting with anti-FLAG or anti-HA. (**G**) FLAG-tagged human Bcl6 was transfected into HEK293T cells with or without HA-tagged human Prkd2, and whole cell lysates were subjected to immunoprecipitation with anti-FLAG M2 magnetic beads, followed by immunoblotting with anti-FLAG or anti-HA. (**H**) Pulldown assay. FLAG-tagged human Bcl6 was transfected into HEK293T cells, and whole cell lysates were subjected to immunoprecipitation with anti-FLAG M2 magnetic beads. Immunoprecipitates were incubated with recombinant GST-tagged human Prkd2, followed by immunoblotting anti-FLAG or anti-Prkd2. (**I**) FLAG-tagged human Bcl6 was transfected into HEK293T cells with or without HA-tagged human full length or kinase domain-deleted (ΔK) Prkd2. Cell lysates were subjected to Phos-tag or normal immunoblot analysis using anti-FLAG or anti-HA. (**J**) Immunoblot analysis of HA-tagged Bcl6 in whole cell lysates, cytosolic extracts, or nuclear extracts of HEK293T cells transfected with or without FLAG-tagged human full length or kinase domain-deleted (ΔK) Prkd2. α-Tubulin and Histone H3 were used as cytoplasmic and nuclear markers, respectively, and as loading controls (**D-G, I, J**). Data are representative of three independent experiments. At least 5 mice/genotype were used per experiment (mean ± SD in A-C). *P* values were determined by unpaired Student's *t* test (NS: not significant and $^{**}P < 0.01$).

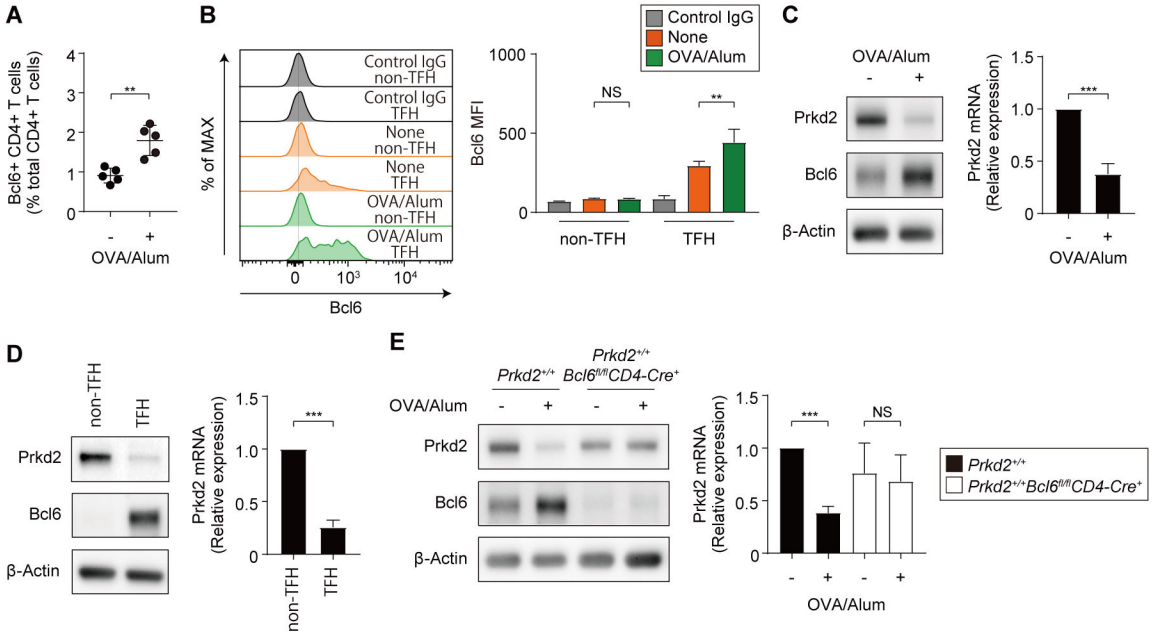

Fig. 5. Bcl6 downregulates *Prkd2* in CD4$^+$ T cells.

(**A**) Frequency of Bcl6 expressing CD4$^+$ T cells (CD3$^+$CD4$^+$Bcl6^{high}) in spleen from unimmunized *Prkd2*$^{+/+}$ mice (−) or from *Prkd2*$^{+/+}$ mice on day 6 after OVA/alum immunization (+). Each symbol represents an individual mouse. At least 5 mice were used per each condition. (**B**) Mean fluorescence intensity of Bcl6 in non-TFH (CD3$^+$CD4$^+$PD-1^{low}CXCR5^{low}) and TFH (CD3$^+$CD4$^+$PD-1^{high}CXCR5^{high}) in spleen from unimmunized *Prkd2*$^{+/+}$ mice (None) or from *Prkd2*$^{+/+}$ mice on day 6 after OVA/alum immunization. Splenocytes from unimmunized mice were used to stain with isotype control IgG. Representative flow cytometric histogram plots (left) and quantification (right). At least 5 mice were used per each condition. (**C**) Immunoblot analysis of Prkd2 and Bcl6 (left), and qRT-PCR analysis of Prkd2 mRNA (right) in splenic CD4$^+$ T cells from unimmunized *Prkd2*$^{+/+}$ mice (−) or from *Prkd2*$^{+/+}$ mice on day 6 after OVA/alum immunization (+). Prkd2 mRNA was normalized to GAPDH mRNA level in CD4$^+$ T cells from unimmunized mice. (**D**) Immunoblot analysis of Prkd2 and Bcl6 (left), and qRT-PCR analysis of Prkd2 mRNA (right) in non-TFH (PD-1^{low}CXCR5^{low}) or TFH (PD-1^{high}CXCR5^{high}) sorted from the same pool of *Prkd2*$^{+/+}$ CD4$^+$ T cells. Prkd2 mRNA was normalized to GAPDH mRNA level in non-TFH. Data for qRT-PCR is average of three independent experiments. (**E**) Immunoblot analysis of Prkd2 and Bcl6 (left), and qRT-PCR analysis of Prkd2 mRNA (right) in splenic CD4$^+$ T cells from unimmunized mice (−) or from mice on day 6 after OVA/alum immunization (+). Prkd2 mRNA was normalized to GAPDH mRNA level in CD4$^+$ T cells from unimmunized *Prkd2*$^{+/+}$ mice. Data are representative of three independent experiments (mean ± SD in A-E). *P* values were determined by unpaired Student's *t* test (NS: not significant, ** $P < 0.01$, and *** $P < 0.001$).

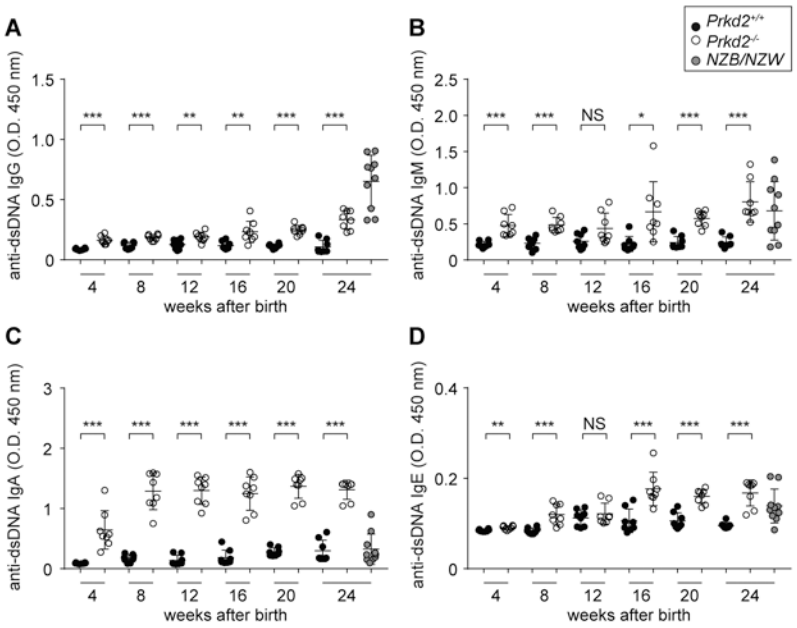

Fig. 6. dsDNA antibodies in *Prkd2*$^{-/-}$ mice.

(**A-D**) dsDNA-specific IgG (**A**), dsDNA-specific IgM (**B**), dsDNA-specific IgA (**C**), and dsDNA-specific IgE (**D**) concentrations in serum from unimmunized 4 – 24 week-old *Prkd2*$^{+/+}$ and *Prkd2*$^{-/-}$ mice. 24 week-old NZB/NZW F1 hybrid mice known to develop autoimmune disease are shown as a positive control. Each symbol represents an individual mouse. Data are representative of three independent experiments with at least 5 mice/genotype (mean ± SD); *P* values were determined by unpaired Student's *t* test (NS: not significant; **P* < 0.05, ***P* < 0.01 and ****P* < 0.001).